




# Robust optimization of aerodynamic loadings for airfoil inverse designs

C. J. B. Reis<sup>1</sup> · N. Manzanara-Filho<sup>1</sup> · A. M. G. de Lima<sup>2</sup> 

Received: 6 September 2018 / Accepted: 25 March 2019 / Published online: 5 April 2019  
© The Brazilian Society of Mechanical Sciences and Engineering 2019

## Abstract

For the modern design of more realistic aerodynamic shapes, disturbances caused by uncertain operating conditions must be conveniently considered, since they can affect significantly the performance of the designed systems. In this situation, the concept of robust design in conjunction with optimization tools is strongly recommended, since the interest is to maximize the performance and its robustness, simultaneously. Clearly, the great number of exact evaluations normally required to compute the robustness makes the robust optimization in aerodynamics computationally prohibitive, particularly when direct methods are chosen. To overcome this drawback, inverse methods appear as an interesting option, provided a robust aerodynamic loading can be furnished previously at low computational costs. However, few works have been dedicated to this subject in the open literature, which motivates the present study. The focus is to apply the robustness concept to optimize the velocity (or pressure) distributions for airfoil inverse designs, using a boundary layer method to predict the aerodynamic coefficients prior to the knowledge of the final airfoil shape. Here, the velocity distribution is parameterized using B-spline polygons with a set of control points, where the design variables are the ordinates of these points in the parameterization. The resulting robust multiobjective optimization problem involves the performance of the airfoil as a first objective function and its robustness introduced as additional objective to be optimized simultaneously. To illustrate the usefulness of the proposed robust design method, an example of drag minimization for an isolated airfoil is addressed and the aerodynamic coefficients for the optimal airfoils are compared with the corresponding obtained by experiments from the open literature.

**Keywords** Aerodynamics · Airfoils · Inverse methods · Robust design · Multiobjective optimization

## 1 Introduction

Nowadays, it becomes clear the substantial progress in the development of high-speed computers and modern digital data processing tools. As a result, some complex real-world aerodynamic problems that were never fully implemented before can now be solved numerically using modern digital

computers [1]. In the quest for optimization tools coupled with computational fluid dynamics (CFD), it is true.

For example, in aerodynamic designs, numerical optimization tools coupled with CFD enable to optimize aerodynamic shapes (turbomachinery cascades, blades, wings, airfoils, etc.) for a desired application, increasing their efficiency during their useful life and reducing significantly the costs of performing a wind tunnel test [2]. However, for more realistic situations in which uncertainties are present, it is not uncommon to see a naive application of numerical optimization tools producing unexpected problems with unacceptable optimal results [1]. Hence, the designed aerodynamic shapes operate efficiently only for the optimized conditions. To overcome this drawback, more recently, the robust design concept in conjunction with multiobjective optimization tools have emerged as a new challenge in the design of aerodynamic shapes. The interest is to provide optimal aerodynamic performances that remain unchanged, even in the presence of

---

Technical Editor: André Cavalieri.

---

✉ A. M. G. de Lima  
amglima@ufu.br

<sup>1</sup> Mechanical Engineering Institute, Federal University of Itajubá, Campus Prof. José Rodrigues Seabra, BPS, 1303, Itajubá, MG CEP 37500, Brazil

<sup>2</sup> School of Mechanical Engineering, Federal University of Uberlândia, Campus Santa Mônica, P. O. Box 593, Uberlândia, MG 38400-902, Brazil

disturbances caused by manufacturing/assembling errors, natural wear or small changes in operational conditions, just to mention a few. Clearly, there exist uncertainties related to the assumptions adopted in the construction of the numerical model [1–4], but in the present study, these uncertainties have not been taken into account in this study.

Classical approaches used to measure the robustness of a set of design variables rely on signal-to-noise ratios (SNR) for determining which variables provoke the higher variations in the response [5]. It requires a full factorial number for the aerodynamic evaluation of a set of design variables or, at least, a Latin-Hyper-Cube sampling [6]. However, in some cases, it becomes prohibitive due to the high computational burden and time associated with the large number of exact evaluations. Gradient optimization methods accounting for noisy variables could be used instead, but the convergence is guaranteed only to local optima [7]. In this work, the search for the optimal and robust airfoil inverse design is based on a multiobjective optimization tool [8–10]. Particularly, it is adopted herein a variant of the Non-dominated Sorting Genetic Algorithm (NSGA II) proposed by Srinivas and Deb [10] and available in the MATLAB's Optimization Toolbox [11]. Based on the interaction between the fitness and robustness functions, the NSGA II algorithm provides compromised solutions or Pareto front of optimal solutions in a two-objective space.

In the quest for the optimal design of aerodynamic shapes, the methods can be generally classified as direct or inverse. The so-called direct methods that act directly on the airfoil geometry for a given set of design variables and, in the sequence, the aerodynamic properties of the airfoil geometry are computed. However, the use of such procedures in conjunction with optimization tools may become practically unfeasible as the number of geometric variables increase. On the other hand, the so-called inverse methods deal with the velocity (or pressure) distributions rather than with the airfoil shape directly. Once the target velocity distributions are constructed (or given), the corresponding airfoil geometry can be found by using inverse numerical optimization tools, with considerably lower computational cost when compared with the direct optimization methods [12]. This feature makes the inverse methods attractive to be used in conjunction with the robust optimization technique proposed herein. However, it requires a second phase regarding the inversion of the velocity (or pressure) distribution into the final airfoil geometry [1].

The inverse design method combined with genetic algorithms tools has been applied by Obayashi and Takanashi [12] for isolated transonic airfoils, but without any attempt to address the issue of robustness. Despite the fact that much research on robust analyses coupled with direct design methods has been carried out in the open literature, few papers [2]

have been addressed the robust design strategies for airfoil inverse designs, which motivates the present study.

Hence, an attempt was made to investigate the multiobjective optimization via NSGA algorithm of inverse design airfoils. One of the objectives to be minimized is the *vulnerability* (inverse of robustness) of the airfoil due to small perturbations introduced in its final geometry. Starting from a baseline airfoil, the aerodynamic loading (velocity distribution) over its suction side is allowed to vary within boundaries in order to form a population that will evolve toward an optimum, according to a desired fitness function. Finally, selected cases of optimized loading are transformed into airfoils shapes and analyzed directly to assess whether the resulting robustness is comparatively like that evaluated inversely and the main features and capabilities of the proposed robust design method are highlighted.

## 2 Description of the optimization problem and the airfoil inverse procedure

### 2.1 Basic methodology

The question to be investigated in this study is whether robust airfoil shapes, meaning shapes that are less sensitive to geometrical variability, can be created by means of a robust multiobjective optimization that seeks for both high performance individuals and individuals that exhibit a low variation in the performance given a disturbance in their geometry. Being an inverse method, the performance and sensitivity analysis are evaluated approximately given only the velocity distribution as a function of the airfoil chord. A multiobjective genetic algorithm is chosen herein for explore that question.

Genetic algorithms simulate natural evolution by selection of the best fit individuals. These individuals are ranked by means of a performance function that, given the characteristics of one individual, produces a score in one or multiple aspects, for respectively single or multiobjective performance functions. These selected individuals have a higher probability of crossing over their characteristics to generate new individuals. Individuals that are not selected have a lower chance to pass on their "genes" and a few (the lower ranking individuals) are eliminated on each generation step. Dependent from the number of parameters (genes) allowed to vary during the optimization process is the size of the population. A large number of parameters means a large population and each individual must be ranked via the performance function. In present study, the velocity distribution on each individual will determine its ability to be selected.

The number of parameters describing the velocity distribution of a two-dimensional isolated airfoil is dependent on the parameterization scheme [12]. A common option is the

use of global Bezier polynomials to represent the velocity curves. However, it has been adopted herein the B-spline scheme [13], since it exhibits a relatively greater flexibility of the curves generated. Additionally, it provides a wider solution space of possible velocity distributions for the present problem.

Figure 1 shows the parametric representation of the velocity distribution over an isolated airfoil, where the lower and upper curves represent the pressure side and suction side of the airfoil, respectively. By conveniently moving the control points, the resulting curve follows a smooth convex hull. Hence, these control points can be used to represent the velocity distribution, providing a straightforward strategy to define the individuals of the population in the optimization phase.

The methodology employed herein is described as follows:

- (1) A baseline airfoil is selected, based upon its response for the desired application: general aviation, wind turbines, turbomachinery, etc.;
- (2) For a given design angle of incidence, the velocity distribution around this baseline airfoil is obtained (via a physical model or a numerical simulation, for instance) and tabulated as a function of the normalized boundary layer length, or the normalized length from the stagnation point to the trailing edge. The velocity distribution is then interpolated into a B-spline function, with a selected number of control points (as an example, see Fig. 1);

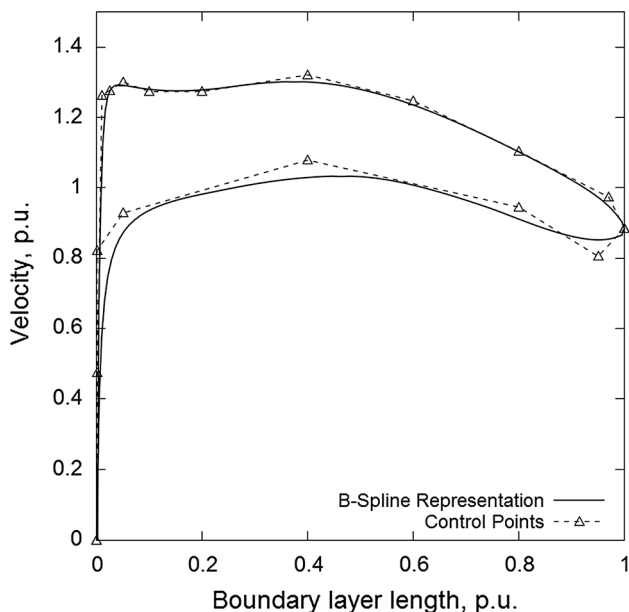


Fig. 1 B-spline parameterization of the velocity distribution and the control points

- (3) For an application, geometrical errors are introduced in the original airfoil shape. For example, dirt build-up on gas turbine compressor blades and vanes, economical manufacture (airfoil shape precision) on low cost applications, ice deposition on wings. For the disturbed shapes, the velocity distribution is obtained (again, via a physical model or a numerical simulation), tabulated and also mapped into B-splines. The deviation of the control points to the baseline velocity distribution is used to give an idea of the order of magnitude of the amount to be added or subtracted from the control points in the individuals to be ranked by the performance function during the genetic algorithm optimization;
- (4) Upper and lower ranges of variability for each control point are determined with the aim of allowing the control points to generate the majority of the possible distributions of velocity due to the geometry variation;
- (5) Based on the number of variables (control points) to be optimized, the initial population is generated within the variability ranges set on the previous step, and the genetic algorithm will simulate the evolution until stabilization or a maximum number of generations is achieved. The evolution of the performance function estimates the main objective (low drag, high lift-to-drag ratio, or another suitable performance indicator), and the variability of the main objective when subjected to the application of a known group of disturbances, one at a time;
- (6) The resulting Pareto front is verified, and a few individuals are manually selected to be inverted to geometry and for evaluation of their properties.

### 2.2 Performance index for the robust optimization problem

As stated by Kumar et al. [14], the robust design optimization in aerodynamics can be formulated as a multiobjective optimization problem in which both the expectation and variance of a performance index are minimized simultaneously. For the robust multiobjective optimization problem considered herein, where the drag,  $C_d$ , and its related standard deviation,  $\sigma_{C_d}$ , are to be minimized simultaneously by means of a multiobjective optimization tool, a possible performance index can be given by:

$$J(\mathbf{y}) = \min[C_d, \sigma_{C_d}] \tag{1}$$

where  $\mathbf{y}$  is the vector containing the design parameters,  $C_d$ , is the drag coefficient, and  $\sigma_{C_d} = \sqrt{\sum_{k=1}^N (C_{d_k} - \bar{C}_d)^2} / N$  is its standard deviation, which is considered herein to be equal to the vulnerability.  $N$  indicates the number of samples of the perturbed velocity distribution of an individual.

Instead of  $C_d$ , another performance characteristic could be used (lift, lift-to-drag ratio, and so on).

To address the optimization problem (1), the lower and upper velocity limits (as defined in Table 1), the pressure side velocities, the required lift  $C_l$ , and airfoil thickness  $t$  have all been specified. Also, the number of inflection points on velocity curves is required to be lower than 2, to avoid excessive undesirable oscillations in the resulting shape (as per Obayashi and Takanashi [12]; see also Drela [15] for further examples with inverse design airfoil optimization). The constraint relation,  $dC_{p,s}/dx \leq 2.5$ , has been imposed, where  $C_{p,s}$  is the pressure coefficient on the suction side of the airfoil. The airfoil thickness  $t$  is approximated by [12]:

$$t = \left( \sqrt{1 - M_\infty^2} / 2 \right) \int_0^1 [(C_{p,p} + C_{p,s}) / 2] dx \tag{2}$$

where  $M_\infty$  is the Mach number of the free stream and  $C_{p,p}$  is the pressure coefficient distribution on the pressure side of the airfoil.

The Squire–Young equation in its reduced form [16, 17] has been also used to relate the momentum thickness provided by the boundary layer method with the potential velocity at the trailing edge. It enables to estimate the viscous drag as:

$$C_d = 2\Theta_{te} (U_{te} / U_\infty)^{3.2} \tag{3}$$

where  $\Theta_{te}$  is the momentum thickness at the trailing edge normalized by the airfoil chord, and  $U_{te}$  and  $U_\infty$  are, respectively, the trailing edge and free stream velocities.

It is important to emphasize that Eq. (3) is valid only for incompressible flows, which is the situation focused on this work, corresponding to,  $M_\infty = 0$ , in Eq. (2).

### 2.3 Airfoil inversion procedure

For the inverse design itself (i.e., to find the airfoil shape knowing the velocity distribution), one uses herein an improved version of the controlled random search (CRS) evolutionary algorithm, known as CRS-VBR, proposed initially by Manzanares-Filho et al. [18]. The problem is based on a single objective function to be minimized, which represents the differences between the optimized velocity distributions and the velocity distributions for the searched airfoil geometry. To verify the airfoil shape, a two-dimensional Martensen-derived vortex panel method has been used [19]. Also, a “fairing-in” correction of the trailing edge flow has been performed to reduce the errors due to the lack of the viscous flow and transpiration effects in the vortex panel method, as detailed by Gostelow [20] and implemented by Manzanares-Filho [21].

The velocity distribution resulting from the vortex panel method is split at the stagnation point and the lengths of the suction and pressure sides are normalized for comparison purposes with the desired distribution. The number of panels used was 120 with a finer discretization near the leading and trailing edges. The angle of attack was forced to be close to the angle of the baseline airfoil within a hundredth of a degree.

It is emphasized that the inversion method implemented herein is independent from the optimization phase. Therefore, more efficient and reliable methods (of higher fidelity) could be used, if available. Here, the results obtained were within 0.1% average error between the required aerodynamic loading and the corresponding one produced by the airfoil geometry found. Thus, in terms of applicability, the proposed inverse method used to reconstruct the airfoil geometry is intended to be acceptable.

## 3 Description of the example

### 3.1 Main setup, boundary layer methods and NSGA II

For the example addressed herein to verify the methodology described above, it will be used as baseline the laminar airfoil NACA 65<sub>1</sub>-412 in the optimization phase. Only the velocity distribution on the suction side of the airfoil is varied and the abscissa of the control points are fixed. A total of 12 control points are retained in the parameterization scheme, where the first point indicates the stagnation point of the airfoil, fixed at the origin with abscissa equal to 0, and the last one, with abscissa equal to 1, coincides with the velocity at the trailing edge (also fixed). Thus, a total number of 10 design variables (ordinates) can vary within their lower and upper admissible limits, as indicated by the

**Table 1** Admissible variations of the control points for the velocity distribution

Abscissa (x)	Ordinate (y) (suction side)	Lower limit	Upper limit	Admissible variations
0.001	0.475	0.47	0.48	0.01
0.010	1.260	1.00	1.50	0.50
0.025	1.280	1.10	1.50	0.40
0.050	1.300	1.10	1.50	0.40
0.100	1.270	1.10	1.50	0.40
0.200	1.270	1.10	1.50	0.40
0.400	1.320	1.10	1.50	0.40
0.600	1.240	1.10	1.40	0.30
0.800	1.100	1.00	1.20	0.20
0.970	1.000	1.00	1.10	0.10

dashed lines depicted in Fig. 2. Table 1 shows the lower and upper limits of the 10 design variables (velocity ordinates of control points) used herein to generate the initial population and its evolution along the optimization process.

The upper limits were adjusted to fit the solution to one that is not so far from the original velocity distribution, especially near the airfoil trailing edge. To avoid the occurrence of curvature discontinuity at the leading edge of the resulting airfoil after inversion from velocity distribution to geometry, the limits of the second control point located at the  $y$  axis are set quite close, to prevent it from moving from the suction side to the pressure side. Also, unlike classical representations of velocity distributions, where the abscissa are generated in terms of percentages of the airfoil chord, here, the abscissa of the distribution shown in Fig. 2 were normalized by the boundary layer length.

The drag  $C_d$  has been computed by using the integral boundary layer methods using the known velocity distributions of an individual as input. The laminar portion of a boundary layer is computed by applying the so-called Thwaites' method and the transition is predicted by the Michel criterion and the turbulent portion is estimated by the Head method [22], respectively. The authors understand that these criteria are semiempirical and may be subjected to criticism. But, as they will be applied uniformly and systematically to all individuals, it becomes possible to perform a comparative study.

The samples used to evaluate the standard deviation of the optimal solutions have been obtained by adding/subtracting from each control point ordinate (design variable)

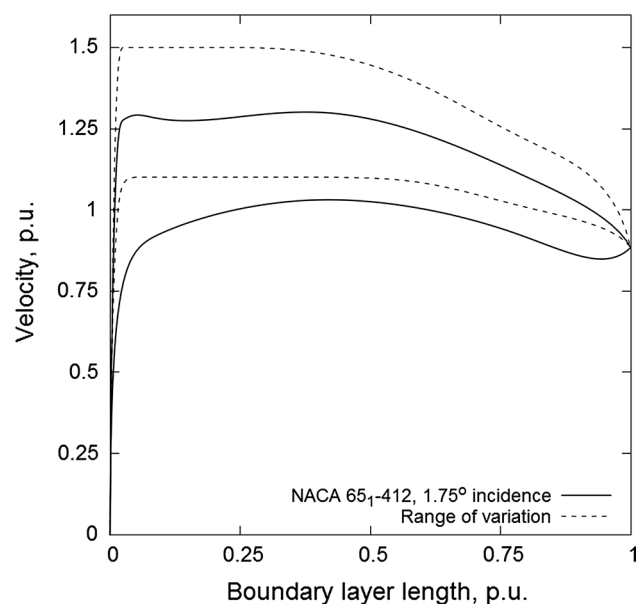


**Fig. 2** Variations of the suction side for the population in the optimization

a percentage ( $\pm 5\%$ ) of its allowable range of variations (seen in the last column of Table 1). In this way, a set of 20 disturbed velocity distributions (two times the number of design variables) have been generated for each individual. Note that, the amount of the perturbation is dependent on the abscissa of the control point. Since these abscissas are the same for all the individuals, it provides a way to perform a comparative measure of the deviation from the non-perturbed state between individuals.

In the quest for penalizations, for the equality constraints, airfoil thickness,  $t$ , can vary from,  $\pm 5\%$ , of the baseline airfoil, and the lift,  $C_l$ , should not be more than,  $5\%$ , lower than the baseline airfoil. For the inequality constraints, a violation of the inequality leads to an automatic penalization on the individual. If the calculated value, Calc, is greater or smaller than the specified value, Spec, a penalty factor of,  $F_p = 10$ , is applied, according to the first objective related to the minimization of the drag:

$$C_d = C_d + F_p |1 - \text{Calc}/\text{Spec}| \quad (4)$$

For the search for the optimal and robust solutions, the authors found convenient to use a variant of the so-called Non-dominated Sorting Genetic Algorithm (NSGA II) [10], available in the MATLAB's Optimization Toolbox [11], which provides a set of compromise optimal solutions known as Pareto front. Since none of the non-dominated solutions in the Pareto front can be considered as better than the others, the final decision about the best design solution to be implemented is made a posteriori, accounting for the user's preferences.

It should be mentioned that, the performance index defined by Eq. (1) was programmed in FORTRAN 95 and coupled with NSGA II algorithm in MATLAB code using a set of MEX interface subroutines. The number of populations was of 15 times the total number of design variables, which is 10, resulting in a population of  $N = 150$  individuals in each generation. The renovation rate was adopted as 100%, crossover function was chosen as "scattered" and the mutation function chosen as "uniform," with a ratio of 0.05. Other parameters used the default settings for MATLAB multiobjective genetic algorithm for example: the stopping criterion of average change in the spread of the Pareto front over 100 generations below  $10^{-4}$  and the Pareto fraction of 35%. The Pareto fraction and the distance function control the elitism in the MATLAB implementation of NSGA II [23]. All calculations have been performed in a modern digital computer model Intel Core i7-6700K CPU @ 4.00 GHz, 16 GB RAM, 64 bits.

### 3.2 Numerical results and discussions

To demonstrate the main features and capabilities of the robust optimization method for airfoil inverse designs, the



chosen baseline airfoil NACA 65<sub>1</sub>-412 was tested with angle of attack 1.75°, Reynolds number  $6 \times 10^6$  and incompressible flow ( $M_\infty = 0$ ). Also, the boundary layer transition points were allowed to vary according to the Michel’s criterion.

Figure 3a shows a typical evolution of the population in the objective space using for clarity only a few selected generations: 1st, 30th, 60th, 90th and 103th, which was the last (i.e., the “spread of Pareto front” criterion was satisfied with 103 generations with a total of 15,450 evaluations of the objective functions). Figure 3b shows a zoom close to the resulting Pareto front. The agglomeration of points of

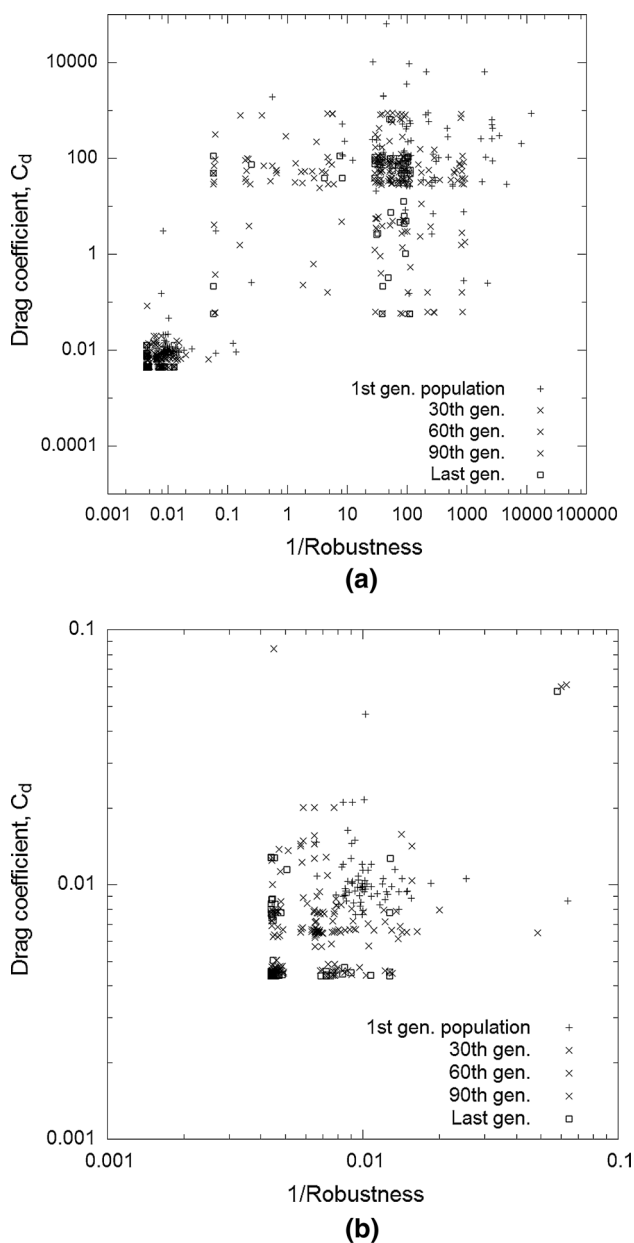


Fig. 3 a Typical evolution map of the population. b A zoom close to the resulting non-dominated set (Pareto front)

previous generations and the last one indicates a convergence trend. It is important to emphasize that getting the true Pareto front is not a prime objective here, but rather to get substantially improved solutions at the capability level of NSGA II algorithm with the adopted parameters.

The resulting front of Pareto optimal solutions is better shown in Fig. 4. It is observed the appearance of two distinct groups of airfoils, called herein as families 1 (low drag front) and 2 (drag plus penalty). The obtained characteristics for the baseline and selected airfoils are given in Table 2.

In Fig. 5, the velocity distributions and geometries for family 1 (airfoils A1, B1, C1 and D1) are plotted after the inversion of the velocity profiles. It can be noted a progressive trend toward a more blunt peak for the airfoil D1, when compared to airfoil A1. It demonstrates a sharp velocity increasing followed by a plateau, which resembles a supercritical airfoil. This plateau causes the speed to decrease more steeply toward the trailing edge than on the airfoils B1, C1 and D1. Also, it will control the boundary layer growth for a big portion of the airfoil, but it is also expected that the following steeper negative gradient will be more sensitive to small perturbations. It is in perfect agreement with

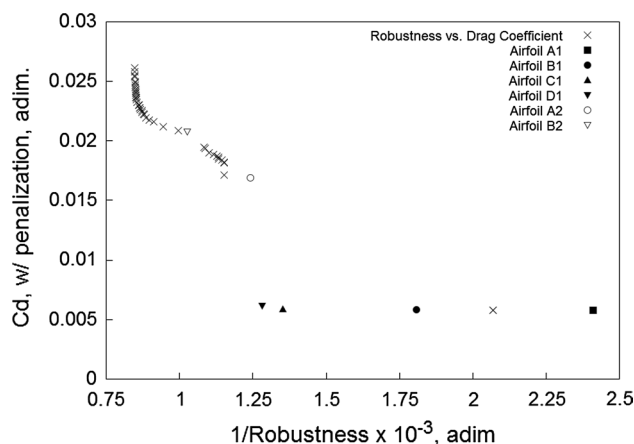


Fig. 4 Pareto front for the robust optimization problem

Table 2 Characteristics for baseline and families 1 and 2 airfoils

Airfoils tested	$t$ , %chord	Incidence (°)	$C_l$	$C_d$	$\sigma$
NACA 65 <sub>1</sub> -412	12.0	1.75	0.54	0.0049	–
A1	11.4	1.76	0.56	0.0055	$2.41 \times 10^{-4}$
B1	12.1	1.76	0.54	0.0058	$1.81 \times 10^{-4}$
C1	12.1	1.76	0.54	0.0059	$1.35 \times 10^{-4}$
D1	12.7	1.76	0.54	0.0061	$1.28 \times 10^{-4}$
A2	13.3	1.74	0.55	0.0051	$1.24 \times 10^{-4}$
B2	11.4	1.76	0.54	0.0060	$1.03 \times 10^{-4}$

the relative position of these airfoils in the front of Pareto optimal solutions shown in Fig. 4, where the robustness of airfoil A1 is lower than the other airfoils in that family.

Figures 6 and 7 enable to compare the Pareto optimal solutions for the families 1 and 2 of airfoils in terms of their drags and their associated robustness, calculated for

the obtained geometrical shapes. The obtained geometry was also fit in the form of B-splines, in order to use the same process of measuring the vulnerability of the airfoils, adding a perturbation to the ordinate of each control point in the suction side and calculating the standard deviation of the drag.

Fig. 5 Family 1 airfoils

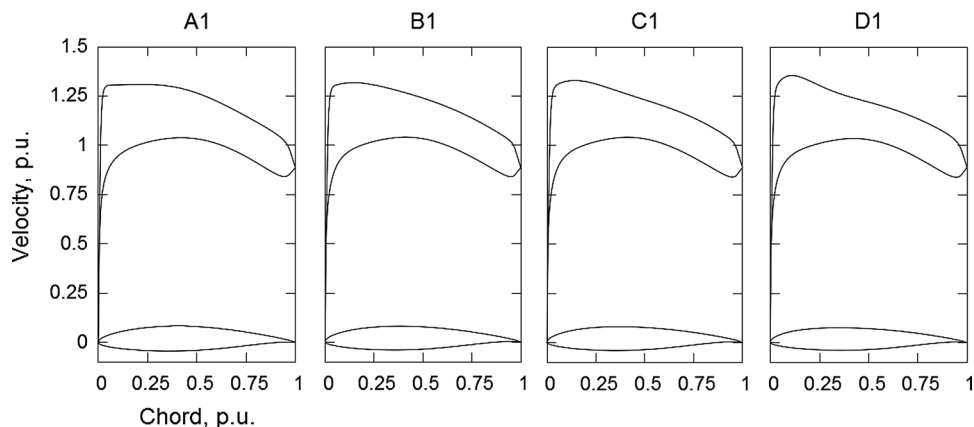


Fig. 6 Robustness to geometrical and angular variations—family 1

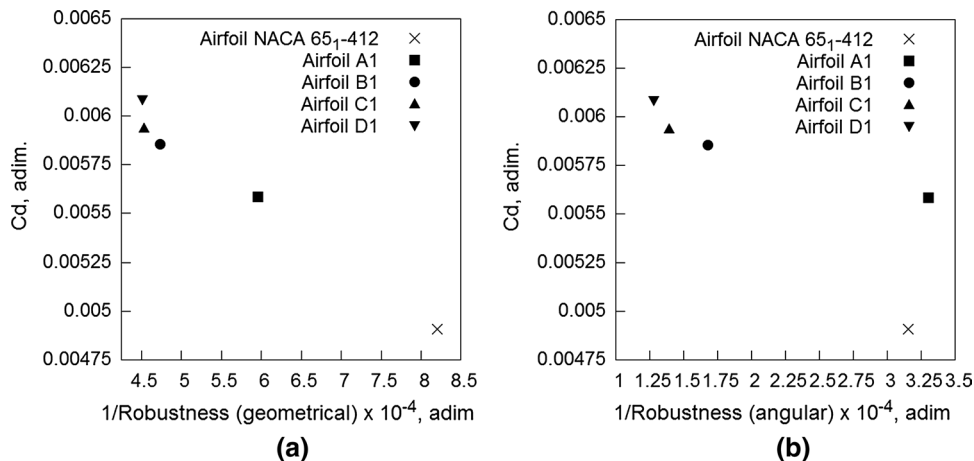
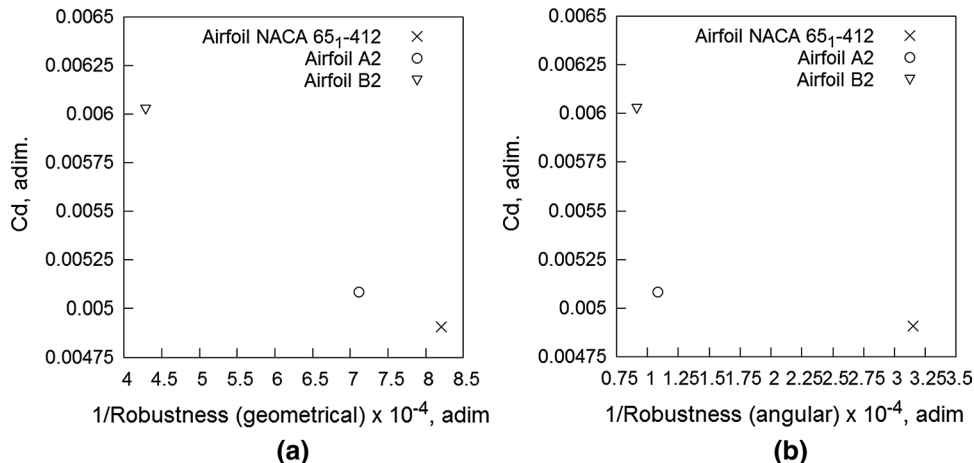


Fig. 7 Robustness to geometrical and angular variations—family 2



These results correspond to a variation of 2% of the chord, applied to the ordinates of the control points defining the suction side geometry (see Figs. 6a and 7a). A total of 10 control points in the suction side were used for stability in the inversion process and 8 were allowed to vary, therefore producing 16 disturbed geometries. A perturbation on the incidence was also applied separately in order to investigate its influence on the performance robustness. A variation of  $\pm 0.5^\circ$  was applied on the angle of attack and for comparative purposes; the same boundary layer subroutine has been used in both inverse and direct calculations.

In the same figures, the perturbed NACA 65<sub>1</sub>-412 is also shown. By examining Figs. 6a and 7a, it is possible to conclude that, for the same level of geometrical perturbation, the airfoils follow the same founding shown in Fig. 4. It implies that, the relative robustness is maintained after the inversion process. The non-dominance of the optimal solutions was also maintained, meaning that, for some loss in one of the objectives (the drag of the airfoil), the second objective (the drag standard deviation) reduces in front of the applied geometrical perturbations.

Figures 6b and 7b show the influence of the incidence (angle of attack) on the angular robustness of the airfoil shapes found after the inversion step. It can be noted that, for both airfoil families, these results are in perfect agreement with those appearing in Fig. 4. However, it should be noted that, the inverse method proposed here is not able to completely separate the geometric and angular robustness characteristics of the airfoil in advance. Note that, the flow incidence is unknown in the first step regarding the robust optimization of the velocity distribution. Therefore, only after performing the inversion geometry in the second step, it is possible to evaluate the relative influence of these separate effects to decide which airfoils meet the design requirements. A possible way to consider these effects beforehand is to apply the thin airfoil theory in order to compute the fitness function. However, it should be reminded that, such a theory only leads to an estimation of the effects of airfoil curvature and angle of attack on the velocity distribution, as well as an estimation of the airfoil thickness and lift coefficient.

Now, the designer can make a decision among the available optimal solutions in the Pareto front for an application of interest. For example, if disturbances on the airfoil shapes caused by manufacturing or assembling errors can be controlled, lower drag airfoils are a good choice in this case. But, if it is too difficult to be dealt with, a less sensitive airfoil should be more interesting, with a price to be paid in aerodynamic performance.

For both airfoils of family 2, the penalization strategy defined by Eq. (4) has been not fully effective in the minimization of the drag coefficient during the multiobjective optimization. From Table 2, it can be noted that, the thickness of airfoil A2 remains above the 5% allowed. For

airfoil B2, the violation of its thickness has been irrelevant, as it is not apparent in Table 2, but the minimum number of inflections of the velocity curve was exceeded. Nevertheless, these shapes still achieve reasonably good indexes of drag coefficient and its robustness. Although slightly thinner than allowed, airfoil B2 shows an excellent robustness characteristic. Airfoil A2 is 6% thicker than allowed, but it leads to a very low drag coefficient. Clearly, it should be recognized that, the penalization scheme adopted herein is considered a weak point of the proposed robust optimization for airfoil inverse design.

In the quest for computing time, limits were applied to the number of individuals on the Pareto optimal solutions and on the population size. However, the elimination of non-compliant individuals can reduce the overall diversity of the population, excluding some potential individuals that could evolve into better airfoil shapes. Also, since the Pareto front is formed by a set of compromise solutions, care must be taken in the choice of the penalty function to avoid the reduction of the diversity of the population.

The airfoil shapes shown in Figs. 5 and 8 cannot be well distinguished. Thus, a shape comparison between the optimized airfoils of low drag A1 (less robust) and C1 (more robust) is shown in Fig. 9 by increasing the ordinate scale. In the same figure, it is also shown the base airfoil NACA 65<sub>1</sub>-412 to enable comparisons. From airfoil A1 to C1, one can see a change in the maximum thickness point to a position closer to the leading edge. It speeds up the boundary layer transition, which in turn, causes an increase in the drag coefficient, but also in robustness. For the robustness of the incidence, it can be clearly perceived that, airfoil A1 is closer to the base airfoil, while airfoil C1 is much more robust, as demonstrated by the results appearing in Fig. 6b.

Figure 10 enables to compare the lift–drag curves (drag polar) for the NACA 65<sub>1</sub>-412 and C1 airfoils. The experimental data for the base airfoil were taken from Abbot and von Doenhoff [24]. It is noteworthy that, in the predominantly laminar flow regime (before the so-called *bucket*, characteristic of laminar airfoils), the model is more pessimistic than the experimental results (greater drag values), while in the predominantly turbulent flow regime (after the *bucket*), the model underestimates the actual drag values. However, it does not invalidate the inverse robust optimization methodology proposed herein, since the main feature of the method is exactly to increase the robustness caused by the decrease of this laminar-turbulent transition bucket. It is a delicate point, noting that there could be a great dependence on the transition model used. Since the Michel's transition criterion has been "calibrated" by means of experimental data, like those reported in [21], the calculated results shown in Fig. 10 for the baseline airfoil reproduce satisfactorily the transition bucket.



Fig. 8 Family 2 airfoils

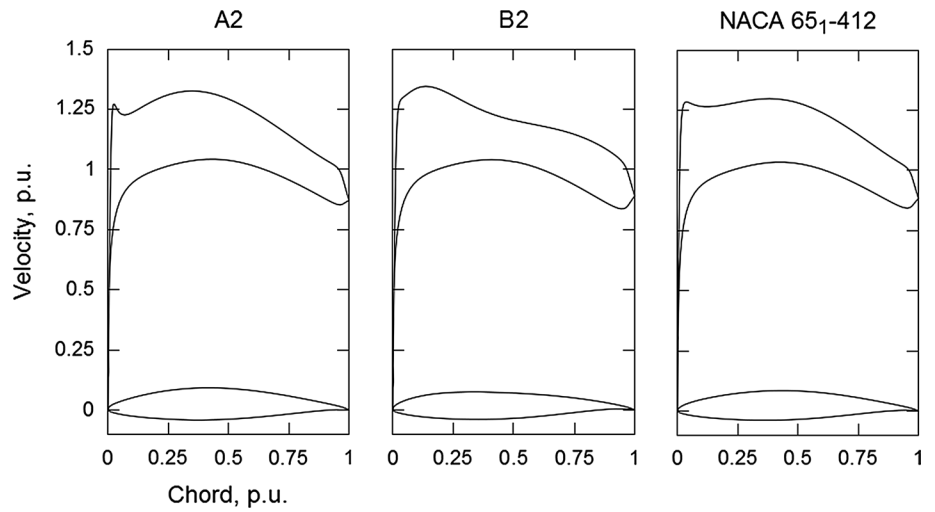


Fig. 9 Shape comparison between NACA 65<sub>1</sub>-412, A1 and C1 airfoils (y axis magnified for clarity)

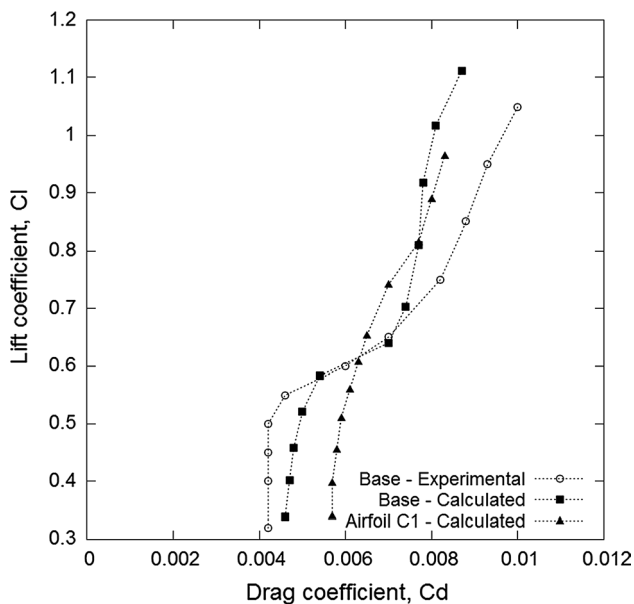
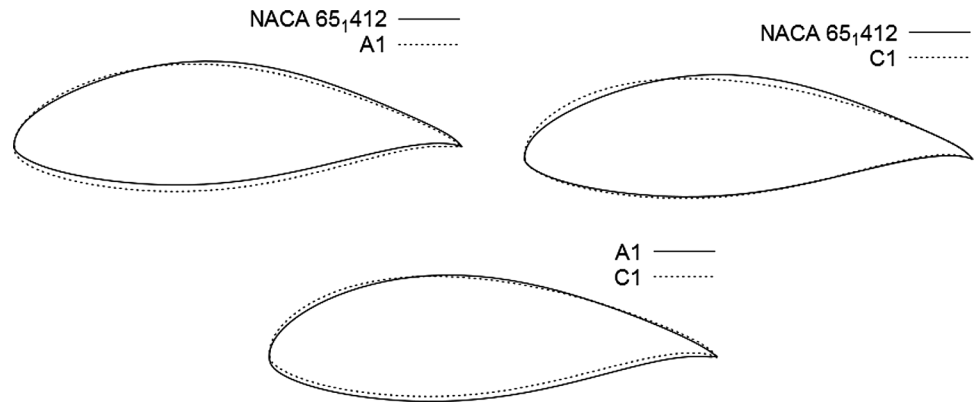


Fig. 10 Comparison between the polar curves for  $Re = 6 \times 10^6$

Note that, for the Reynolds value adopted in this study, this abrupt transition phenomenon occurs at values of  $C_1 \approx 0.54$ , which corresponds to an angle of attack close to  $1.75^\circ$ . For this reason, this value was adopted for carrying out the optimization process. That is, one has chosen the incidence in which the performance of the base airfoil is less robust and applied the proposed inverse optimization methodology in order to find airfoils shapes that are more robust. From Fig. 10, it can be also perceived that the characteristic laminar-turbulent bucket of NACA 65<sub>1</sub>-412 was eliminated in airfoil C1: This optimized airfoil becomes more robust at the cost, however, of a higher drag coefficient in the nominal condition of  $C_1 = 0.54$ .

In order to check whether the accuracy of the direct calculation could be improved, other two CFD alternatives were employed for aerodynamic evaluation: (1) the viscous-inviscid interaction code MSES [25], which employs an  $e^n$  laminar-turbulent boundary layer transition criterion (MSES default options were chosen). (2) The finite volume ANSYS Fluent software (version 16.0), with the Langtry-Menter

4-equation transitional SST turbulence model (employing 2D unstructured meshes with 489,013 triangular volumes and 253,659 nodes, and  $y^+ < 1$  for the nodes closest to the walls). Note that the transitional issue is of paramount importance here since it relates to the robustness requirements. Turbulence models with poor predictive capabilities of boundary layer transition are not eligible here.

Figure 11a compares the polar curves for the base airfoil NACA 65<sub>1</sub>-412 obtained by the two chosen CFD alternatives, by the simplified boundary layer method employed

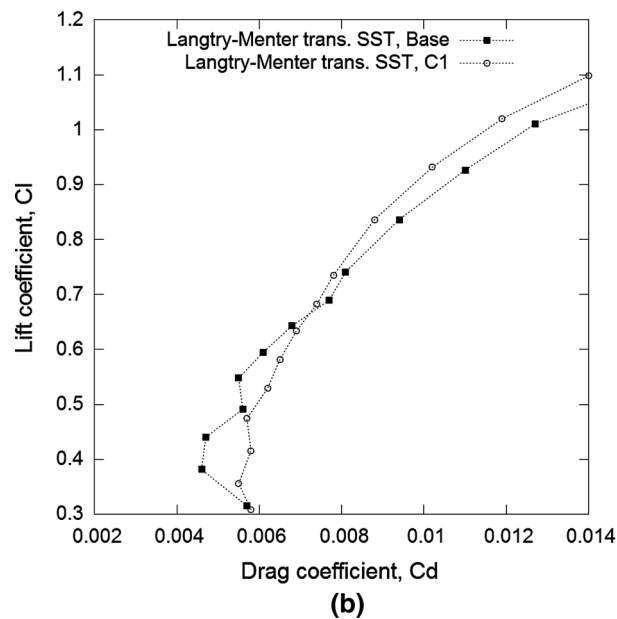
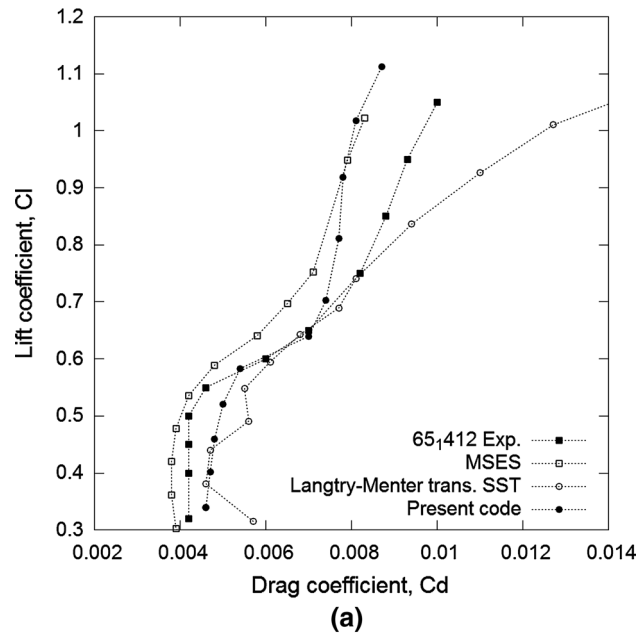


**Fig. 11** **a** Polar curves for the base airfoil NACA 65<sub>1</sub>-412. **b** Polar curves for the base and C1 airfoils using Langtry–Menter 4-equation transitional SST model ( $Re = 6 \times 10^6$ )

during the inverse step (present code) and experimental results. One observes that the results obtained by the three calculation methods present marked differences. Qualitatively, both MSES and the present code captured reasonably the transition bucket shape. However, the present code represented better the sharp transition location than MSES code, which underestimates the drag values over all the bucket range (as compared with experimental results). On the other hand, the Langtry–Menter model produced unstable values of drag for low incidence angles in relation to the sharp transition and overestimated the drag coefficient for higher lift coefficients in the tests performed. Even though its accuracy has not fully met the expectations, the Langtry–Menter model was also able to predict the absence of the transition bucket for the airfoil C1, as one can see in Fig. 11b. This figure also shows that the model produced lower instabilities for the C1 airfoil than for the base airfoil, in low incidence angles. Thus, all the calculation tools were able to capture the expected robustness increase indicated by the proposed inverse methodology in the case of C1 airfoil.

Finally, it is important to highlight that, for this example, the NSGA II was not able to detect Pareto solutions with lower drag in comparison with NACA 65<sub>1</sub>-412 (see Table 2). On the other hand, as already discussed, it was possible to obtain a solution like the airfoil C1, which is significantly more robust (with lower vulnerability) without much drag increase. It was verified by the results of direct geometrical and angular variations shown in Fig. 6. However, it is possible that solutions with lower drag could be obtained using other ranges for the design variables and other parameters of the optimization algorithm. Nevertheless, such solutions would probably be as vulnerable (less robust) as NACA 65<sub>1</sub>-412.

## 4 Concluding remarks

This work proposed a low cost multiobjective optimization methodology to construct robust aerodynamic loadings for two-dimensional airfoil inverse designs. The motivation was to verify whether the final airfoils shapes obtained after geometric inversion could keep the robustness characteristics of the optimized aerodynamic loadings. Within this aim, a two-step methodology has been suggested herein. In the first step, a simple and computationally inexpensive integral boundary layer method was used to assess the nominal aerodynamic performance index of the individuals. In this case, the velocity distribution around the airfoil was parameterized by using B-splines curves and the ordinates of a selected group of control points were considered as design variables. A first objective was to optimize a chosen aerodynamic coefficient—in this work, the minimization of the drag coefficient was chosen. A second objective was to

minimize a vulnerability measure (inverse of the robustness measure). Perturbations were applied to the nominal velocity curves on the airfoil suction side to estimate their robustness measures. The multiobjective algorithm NSGA II was used herein in order to generate the Pareto front, containing the fittest velocity distributions. In the second step of the proposed methodology, some of the compromise solutions in the Pareto front were chosen and subjected to an inverse algorithm to find their associated shapes. In the sequence, the interest was to evaluate the robustness of the airfoils shapes due to small perturbations introduced on their geometry and angle of attack to verify whether the final airfoils shapes were able to keep their robustness in comparison with the pre-optimized robust loadings.

Based on the numerical applications performed herein, it is possible to perceive that, in fact, the final airfoils shapes corresponding to selected individuals in the Pareto front have kept their robustness (both angular and geometrical) due to the perturbations. In other words, robust loading distributions can really produce robust shapes. Firstly, this conclusion seems to be very promising, since it implies that, the aerodynamicist community may benefit of an effective robust optimization strategy for airfoil shape design at a low computational cost. However, a drawback of the methodology should be pointed out: For a certain robust optimal velocity distribution, it is not possible to determine a priori whether the resulting airfoil shape will be more affected by geometric or angular perturbations. Also, as some geometrical and performance constraints like thickness and lift can only be evaluated approximately during the optimization process, it is too difficult to assess whether the shapes to be generated will possess the required characteristics. In this case, the thin airfoil theory could be applied to mitigate this weakness.

A timely perspective in this way is to use a Navier–Stokes solver to evaluate the resulting airfoil shapes computed in the inverse step of the methodology (second step). However, it is expected that, it will certainly require a higher computational effort, but it is still relatively affordable as long as a boundary layer solver of low cost remains active during the robust optimization of the aerodynamic loadings (first step).

**Acknowledgements** The authors are grateful to the FAPEMIG for the financial support to their research projects APQ-01865-18 (N. Manzaneres-Filho) and PPM-00548-18 (A.M.G. de Lima) and the Brazilian Research Council—CNPq for the continued support to their research work, especially through research projects 302026/2016-9 (A.M.G. de Lima). The authors would also like to thank Mr. L.L.F. Soares (a doctorate student at UNIFEI) for his invaluable help with CFD calculations using ANSYS Fluent.

### Compliance with ethical standards

**Conflict of interest** The authors declare that they have no conflict of interest.

## References

- Kontoleonos EA, Giannakoglou KC, Koubogiannis DG (2005) Robust design of compressor cascade airfoils using evolutionary algorithms and surrogate models. In: Proceedings of the 1st international conference on experiments/process/simulation/optimization (IC-EpsMsO), Athens
- Reis CJB, Manzaneres-Filho N, de Lima AMG (2016) Robust optimization of turbomachinery cascades using inverse methods. *J Braz Soc Mech Sci Eng* 38:297–305
- Huysse L, Lewis M (2001) Aerodynamic shape optimization of two dimensional airfoils under uncertain operating conditions. ICASE Report No. 2001-1, ICASE, NASA Langley Research Center, Hampton, Virginia, USA
- Sampaio R, Soize C (2007) On measures of nonlinearity effects for uncertain dynamical systems applications to a vibro-impact system. *J Sound Vib* 303:659–674
- Taguchi G, Elsayed EA, Hsiang TC (1989) *Quality engineering in production systems*. McGraw-Hill, New York
- Florian A (1992) An efficient sampling scheme: updates Latin-hyper-cube sampling. *Probab Eng Mech* 7:123–130
- Beyer H, Sendhoff B (2007) Robust optimization—a comprehensive survey. *Comput Methods Appl Mech Eng* 196:3190–3218
- Eschenauer J, Koski J, Osyczka A (1990) *Multicriteria design optimization*. Springer, Berlin
- Lee KH, Park GJ (1996) Robust optimization considering tolerance of design variables. *J Comput Struct* 79:77–86
- Srinivas N, Deb K (1993) Multiobjective using non-dominated sorting in genetic algorithms. Technical Report, Department of Mechanical Engineering, Institute of Technology, India
- The Mathworks Inc (2017) Genetic algorithm and direct search toolbox guide. <http://www.mathworks.com/access/helpdesk/help/pdf/doc/gads/gadstb.pdf>. Accessed 04 Nov 2017
- Obayashi S, Takahashi S (1996) Genetic optimization of target pressure distributions for inverse design methods. *AIAA J* 34:881–886
- Rogers D (2001) *An introduction to NURBS: with historical perspective*. Academic Press, San Diego
- Kumar A, Nair PB, Keane AJ, Shahpar S (2008) Robust design using bayesian Monte Carlo. *Int J Numer Methods Eng* 73:1497–1517
- Drela M (1998) Pros and cons of airfoil optimization. *Front Comput Fluid Dyn*. [https://doi.org/10.1142/9789812815774\\_0019](https://doi.org/10.1142/9789812815774_0019)
- Squire HB, Young AD (1938) The calculation of the profile drag of airfoils. Aeronautical Research Committee, Repts. and Memoranda No. 1838
- Young AD (1989) *Boundary layers*. AIAA Education Series. AIAA, Washington, DC
- Manzaneres-Filho N, Albuquerque RBF, Sousa BS, Santos LGC (2018) A comparative study of controlled random search algorithms with application to inverse airfoil design. *Eng Optim* 50:996–1015
- Lewis RI (1991) *Vortex element methods for fluid dynamic analysis of engineering systems*. Cambridge University Press, Cambridge
- Gostelow JP (1984) Cascade aerodynamics. *J Fluid Mech* 153:503
- Manzaneres-Filho N (1994) Axial flow turbomachinery analysis” (in portuguese). Thesis, Instituto Tecnológico de Aeronáutica-ITA, Brazil
- Moran J (1984) *An introduction to theoretical and computational aerodynamics*. Wiley, New York

23. The Mathworks Inc (2019) Multiobjective genetic algorithm options <https://www.mathworks.com/help/gads/gamultiobj-options-effects.html>. Accessed 01 Mar 2019
24. Abbott IH, von Doenhoff AE (1959) Theory of wing sections. Dover Publications Inc, New York
25. Drela M (2007) A user's guide to MSES 3.05. MIT Department of Aeronautics and Astronautics

**Publisher's Note** Springer Nature remains neutral with regard to jurisdictional claims in published maps and institutional affiliations.